Phase-field study of spacing evolution during transient growth

Sebastian Gurevich, Morteza Amoorezaei, and Nikolas Provatas
Department of Materials Science and Engineering, McMaster University, Hamilton, Ontario, Canada L8S4L7
(Received 10 July 2010; revised manuscript received 4 October 2010; published 29 November 2010)

The primary spacing of a dendritic array grown under transient growth conditions displays a distribution of wavelengths. The average primary spacing is shown, both experimentally and numerically, to evolve between characteristic incubation periods during which the distribution of wavelengths remains essentially stable. Our primary spacing results display a gradual transition period from one spacing range to another, consistent with the fact that the abrupt doubling of spacing predicted by Warren and Langer for an idealized periodic array affects different wavelengths of the distribution at different times. This transition is shown to depend on the rate of change in growth speed using phase-field simulations of directional solidification where the pulling speed is ramped at different rates. In particular, for high rates of change of the pulling speed we observe temporary marginally stable array configurations separated by relatively short lived transitions, while for lower rates of change of the pulling speed the distinction between incubation and transition periods disappears.

DOI: 10.1103/PhysRevE.82.051606 PACS number(s): 81.10.Aj

I. INTRODUCTION

Morphology selection has been a central issue in numerous studies of pattern formation in spatially extended nonequilibrium systems. Directional solidification is a well-established paradigm for the study of competitive effects in driven interfacial pattern-forming systems, such as viscous fingering and electrochemical deposition. Understanding the evolution of primary spacing in an extended solidifying array is also important from a technological viewpoint because dendrite spacing is one of the key parameters that control the mechanical properties of cast products. Different array arrangements produce different microsegregation patterns that can influence other processes, such as solidification shrinkage during the late stages of solidification or precipitation of new phases in the solid state.

Directional solidification has traditionally been studied in the context of steady-state growth. A steady-state dendrite array is assumed as an ideal homogeneous arrangement with uniform spacing. It is the state that in principle is approached under constant growth conditions. In practice, when the temperature field, characterized by a gradient G, and the pulling speed V_p are maintained constant from beginning to end, a marginally stable arrangement with a range of primary spacings appears to be attainable. While spacing selection under steady-state conditions is an important academic paradigm, it is not an accurate representation of the conditions in actual casting processes, where the thermal profile and growth rate are commonly interdependent and evolve with time.

Classical theoretical models predicting a nominal primary spacing for a given set of growth conditions are largely heuristic, dependent on fitting parameters commonly associated with assumptions of the geometry of the steady-state dendrite morphology [1–3]. As steady state is not achievable in practical situations, these models cannot be applied directly, and although useful in elucidating important aspects of spacing selection, these models need to assume the morphology of the structure they are trying to predict. It is also not clear whether they hold outside the conditions of the experiments against which they are calibrated.

The notion of a unique spacing selection mechanism has been challenged by the analytical theory of Warren and Langer, who analyzed the stability of idealized steady-state dendritic arrays to a period doubling instability [4,5] and found that an array can be stable over a range of pulling speeds, implying that there is a range of available spacings that can be accessed through different initial conditions, by varying the growth history, or both. Lin *et al.* [6] reported experiments where ramping the pulling speed in different manners resulted in different arrangements with distinct average primary spacing for the same set of final growth conditions. Losert *et al.* [7] reported experiments where, under a gradual change in pulling speed, the average primary spacing remained stable over a range of pulling speeds, consistent with the theory of Warren and Langer. Beyond that range an abrupt transition to a new stable dendritic arrangement, consistent qualitatively but not quantitatively with a period doubling instability, was observed. The deviation from precise period doubling is attributed to boundary effects.

Phase-field theory has emerged in recent years as a promising candidate for a fundamental theory to model solidification microstructures. Phase-field models are appealing because their free-energy functional is constructed from basic thermodynamics and their kinetics from fundamental conservation laws. Moreover, their parameters are identifiable—if not necessarily known—in terms of fundamental material and process parameters. The first simulations to test spacing versus pulling speed in alloys date back to the work of Boettinger and Warren [8] who found that spacing versus pulling speed fell within a range of values. Their use of very small dendritic arrays, however, likely precluded a quantitative comparison with experiments. More recently, phase-field models have become more quantitative when implemented in the so-called *thin interface limit* [9,10] using novel simulation techniques like adaptive mesh refinement [11]. A first step using phase-field models to quantitatively study spacing selection in directional solidification was taken by Greenwood *et al.* [12] in two dimensions and Provatas and coworkers in three dimensions [13]. These works computed the mean steady-state primary spacing of directionally solidified succinonitrile (SCN) alloys and found very good agreement

with two-dimensional (2D) experiments. These studies suggested that, at least for organic alloys grown under steady-state conditions and one class of initial conditions, there exists a crossover scaling function interpolating between two power-law spacing regimes observed experimentally and modeled by geometrical models.

Despite the success of phase-field modeling in predicting steady-state spacing, as well as other steady-state properties such as cell tip structure [14], this formalism has hardly been used to systematically explore spacing under *transient* solidification conditions. In this paper, we exploit the ability of phase-field models to self-consistently simulate topologically complex cell and dendrite structures, kinetics and surface tension anisotropy, phase mobilities, different thermal conditions, and different initial conditions in order to study transient spacing development and how it may relate to previous models and theories of the steady-state solidification structures.

II. PHASE-FIELD MODEL DESCRIPTION

For convenience we focus on simulations that are two dimensional, corresponding to a longitudinal section through a row of dendrites. We consider unidirectional solidification of an AlCu alloy system in the dilute limit with straight solidus and liquidus lines of slopes m/k and m, respectively. The corresponding partition relation is $c_s=kc_l$, where c_s (c_l) is the molar concentration of impurities at the solid (liquid) side of the interface and k is the partition coefficient. Since solute diffusion in the solid is several orders of magnitude lower than in the liquid and convection in the liquid does not significantly affect the final spacing in upward directional solidification [15], both are neglected. Latent heat production is neglected, resulting in the frozen temperature approximation, modeled as $T(z,t)=T_0+G(t)[z-z_0-\int_0^t V_p(t')dt']$, where $T(z_0,0)=T_0$ is a reference temperature, while $G(t)$ and $V_p(t)$ are the local thermal gradient and pulling speed, respectively. A fourfold anisotropy is implemented on the surface energy through the anisotropy function $a(\theta)=1+\epsilon\cos(4\theta)$, where ϵ is the anisotropy strength and θ is the angle between the normal to the interface and an underlying crystalline axis, taken to coincide with the direction of the thermal gradient. Setting as the concentration reference the impurity concentration on the liquid side of an advancing steady-state planar interface $c_l^0=c_0/k$, where c_0 is the nominal alloy composition, we reach the following sharp interface solidification equations:

$$\partial_t c = D\nabla^2 c - \vec{\nabla}\cdot\vec{j}_c, \tag{1}$$

$$c_l(1-k)v_n = -D\partial_n c|_l + \hat{n}\cdot\vec{j}_c, \tag{2}$$

$$c_l/c_l^0 = 1-(1-k)\kappa d_0(\theta)-(1-k)\left(z-\int_0^t V_p(t')dt'\right)/l_T - (1-k)\beta v_n, \tag{3}$$

where $d_0(\theta)=\Gamma(\theta)T_m/L$ is the solutal capillary length, $\Delta T_0=|m|(1-k)c_l^0$ is the freezing range, $\gamma(\theta)$ is the interface energy, $l_T=\Delta T_0/G$ is the thermal length, and $\beta=1/(\mu_k\Delta T_0)$ is the kinetic coefficient. The constants T_m and L are the melting temperature and latent heat of fusion of aluminum.

In order to promote side branching, thermal noise-induced concentration fluctuations are included in the liquid by following Echebarria *et al.* [16] and introducing the current $\vec{j}_c$, whose components are random variables obeying a Gaussian distribution with variance

$$\langle j_c^m(\vec{r},t)j_c^n(\vec{r}',t')\rangle = 2DF_c\delta_{mn}\delta(\vec{r}-\vec{r}')\delta(t-t'), \tag{4}$$

where the magnitude F_c is determined through the fluctuation-dissipation relation

$$\langle(\delta c)^2\rangle = \frac{c}{(N_A/v_0)\Delta V} = \frac{F_c}{\Delta V}, \tag{5}$$

where $\langle(\delta c)^2\rangle$ is the equilibrium average of the square of the departure of the concentration from its equilibrium value in a microscopically large but macroscopically small volume ΔV. The first equality in Eq. (5) follows from the standard relation $\langle(\delta n)^2\rangle=n$, where n is the number of solute atoms in the small volume ΔV while using the definition $c=n/N$ and that the number of solvent atoms in the same volume is $N=\Delta V N_A/v_0$, where N_A is Avogadro's number and v_0 is molar volume of solvent atoms. The second equality (right-hand side) of Eq. (5) is obtained by computing $\langle(\delta c)^2\rangle$ directly from the sharp-interface equations (1)–(4). By the procedure outlined in Ref. [17] this incorporation of noise can be shown to yield the appropriate equilibrium interface fluctuation spectrum in the sharp-interface limit.

Equations (1)–(4) are modeled by adapting the phase-field formulation developed by Karma and co-workers and detailed extensively elsewhere [9,10]. The evolution equations are given in terms of a generalization of the field $\tilde{U}=(c-c_l^0)/[c_l^0(1-k)]$, which represents the local supersaturation with respect to the point (c_l^0,T_0):

$$U = \frac{1}{1-k}\left(\frac{c/c_l^0}{(1-\phi)/2+k(1+\phi)/2}-1\right), \tag{6}$$

with the phase-field variable valued at $\phi=1$ (-1) in the solid (liquid). Their explicit form is given by

$$\tau(\hat{n})\left(1-(1-k)\frac{(z-z_{\rm int})}{l_T}\right)\frac{\partial\phi}{\partial t} = w_0^2\vec{\nabla}[a(\hat{n})^2\vec{\nabla}\phi]+\phi-\phi^3-\lambda(1-\phi^2)^2\left(U+\frac{z-z_{\rm int}}{l_T}\right), \tag{7}$$

$$\left(\frac{1+k}{2}-\frac{1-k}{2}\phi\right)\frac{\partial U}{\partial t} = \vec{\nabla}\left[q(\phi)D\vec{\nabla}U-\frac{w_0}{2\sqrt{2}}\{1+(1-k)U\}\hat{n}\frac{\partial\phi}{\partial t}\right] + \left(\frac{1+(1-k)U}{2}\right)\frac{\partial\phi}{\partial t}-\vec{\nabla}\cdot\vec{J}_u, \tag{8}$$

where $z_{\rm int}\equiv\int_0^t V_p dt'$ is the interface position, $\tau(\hat{n})=\tau_0 a^2(\hat{n})$ is

TABLE I. Material parameters defining the AlCu system. m is the liquidus slope, c_0 is the alloy composition, k is the partition coefficient, D is the diffusivity of impurities in the liquid, Γ is the Gibbs-Thomson constant, and ϵ is the anisotropy strength.

$\lvert m\rvert$ (K/wt %)	c_0 (wt %)	k	D (μm^2/s)	Γ (K μm)	ϵ
3.00	0.34	0.15	3400	0.10	0.02

the kinetic relaxation time, $\hat{n} \equiv -(\vec{\nabla}\phi)/(|\vec{\nabla}\phi|)$ is the unit vector normal to the interface, and the fourfold anisotropy is imposed through $a(\hat{n}) = 1 - 3\epsilon + 4\epsilon[(\partial_x\phi)^4 + (\partial_z\phi)^4]$, where ε is the anisotropy strength. The interpolation function $q(\phi) = (1-\phi)/2$ governs diffusivity across the interface. The fluctuating current $\vec{J}_u$ obeys the correlation

$$\langle J_u^m(\vec{r},t) J_u^n(\vec{r}',t')\rangle = 2Dq(\phi)F_u\delta_{mn}\delta(\vec{r}-\vec{r}')\delta(t-t'), \quad (9)$$

and depends explicitly on the phase field ϕ via the solute diffusivity $Dq(\phi)$. The magnitude $F_u = F_u^0[1+(1-k)U]$ is defined by the relation

$$\langle(\delta U)^2\rangle = \frac{\langle(\delta c)^2\rangle}{(\Delta c_0)^2} \equiv \frac{F_u}{\Delta V}, \quad (10)$$

and the constant noise magnitude,

$$F_u^0 = \frac{kv_0}{(1-k)^2 N_A c_0}, \quad (11)$$

is the value of F_u for a reference planar interface at temperature T_0 ($U=0$), while $\Delta c_0 = c_l^0(1-k) = c_0(1/k-1)$ is the concentration jump across the solid-liquid interface.

The material parameters employed are presented in Table I. Kinetic effects are neglected (i.e., $\beta=0$), at least to first order, as shown in [10]. The phase-field equations are simulated using the adaptive-mesh-refinement scheme developed by Provatas and co-workers, details of which can be found in [11,18].

Two different general transient growth conditions are examined in this work. In the first case, direct thermocouple data from a unidirectional solidification experiment [19] were used to extract the local thermal gradient across the solid-liquid interface and the effective front velocity. These were then fitted to provide the functions representing $G(t)$ and $V_p(t)$. In the second case, the thermal gradient is kept constant while the pulling speed is discretely incremented over a predetermined range at varying rates.

Figure 1 shows a typical interface shape and adaptive mesh detail for a subsection of a simulated dendritic array. Following Greenwood *et al.* [12], the primary spacing was extracted through a power spectral analysis of the interface profile. Figure 1 also shows the power spectral analysis of the dendritic structure shown in the top part of the figure. This analysis is typical and reveals a main peak, which corresponds to the mean spacing of the dendritic array as obtained by the usual line intersection or other metallurgical analyses. It also reveals other persistent length scales that may exist in transient data, the norm in most experimental situations.

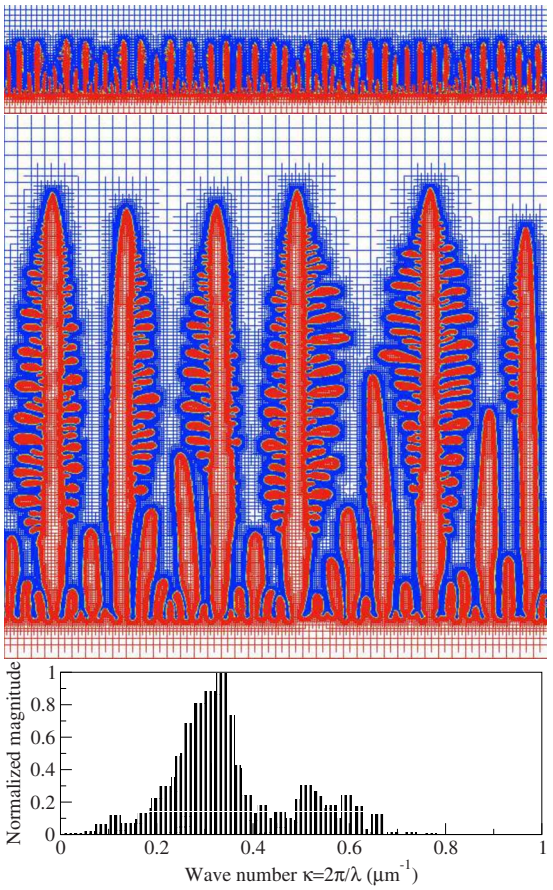

FIG. 1. (Color online) Top two frames show the interface shape of a portion of a typical dendritic array. Grid lines map out the structure of the adaptive mesh. The bottom frame shows the corresponding power spectrum of the interface.

In order to reduce boundary effects we studied the effect of the system size on the primary spacing at steady state conditions. This study, reported in Ref. [19], concluded that the minimum system size required to avoid finite-size effects in simulations is 1 mm. This sets the lower bound of system sizes simulated.

III. RESULTS AND DISCUSSION

A. Transient growth

The time-dependent functions representing the thermal gradient $G(t)$ and pulling speed $V_p(t)$ in the simulations presented in this section were determined by fitting the local thermal gradient across the solid-liquid interface and the effective front velocity obtained from direct thermocouple measurements in the unidirectional solidification experiment reported in [19]. The corresponding plots are shown in Fig. 2. Since the pulling speed was modeled after a fit of the experimental front velocity and the simulated interface is initially positioned at T_L, the simulated front velocity differs from the experimental front velocity used to determine the

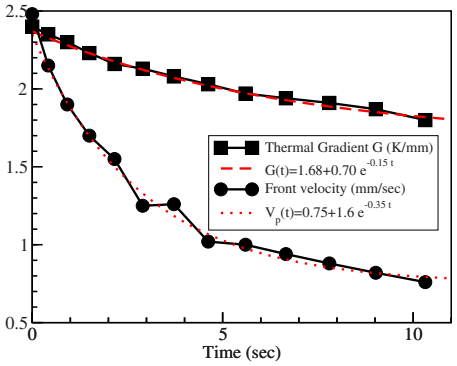

FIG. 2. (Color online) Local thermal gradient across the solid-liquid interface and effective front velocity obtained from direct thermocouple measurements in the unidirectional solidification experiment reported in [19], and the corresponding fitting curves $G(t)$ and $V_p(t)$ employed in the simulations presented in this section.

pulling speed, with the discrepancy decreasing as the system evolves. Figure 3 illustrates three different stages of microstruction evolution using the profiles in Fig. 2. Even though the width of the simulation domain was 2.5 mm, it features only small subsections of the interface to be able to appreciate the details of the interface morphology.

The evolution of the mean spacing in our simulations is characterized by temporary marginally stable states and shows a remarkable qualitative agreement with the new experiments reported in Ref. [19], as shown in Fig. 4. States of nearly stable mean spacing can be (statistically) locally uniform but not globally. Neither existing dendrites are eliminated nor new ones created, although the structure of individual dendrites may change in response to the varying conditions as described in [14]. While the mean spacing remains roughly constant over some time intervals, it may be subject to a slow transverse adjustment process aiming toward global uniformity. The agreement between simulations and experiments is only qualitative since the simulations are two dimensional and, as mentioned, the simulated pulling

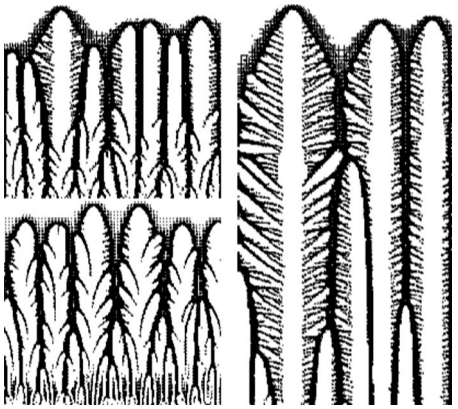

FIG. 3. Details of interface segments of approximately 100 μm width in three different instances of the simulation. At first (bottom left) the interface exhibits kinetic effects due to the initial high velocity, and as the pulling speed decreases the kinetic effects fade (top left). At later time, during a transition period, cell elimination dominates until a new marginally stable state is reached (right).

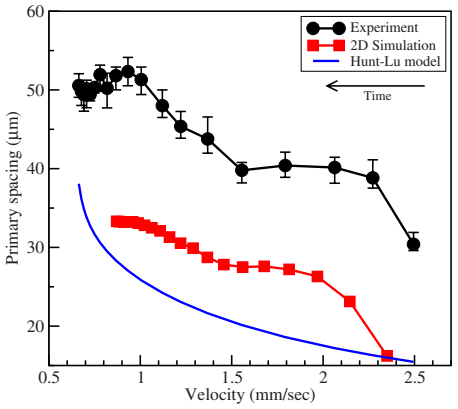

FIG. 4. (Color online) Mean primary spacing as a function of velocity obtained experimentally (black circles) and via 2D phase-field simulation (red squares). The blue curve corresponds to the relationship obtained by Hunt and Lu for unsteady-state solidification. [Note that $G(t)$ is also dynamically changing at each point.]

speed is determined through a fit of the experimentally registered front velocity. It is noteworthy that both results sharply contrast with the monotonic and uniform behavior predicted by geometrical models such as that of Hunt and Lu [20], also included in Fig. 4 for reference.

Analogous dynamics, namely, evolution characterized by temporary marginally stable states, was observed by Losert *et al.* in directional solidification experiments where the pulling speed was slowly ramped [7]. In that case, it was associated with the period doubling instability predicted by Warren and Langer [4,5] even though the mean spacing during the stable states did not differ by a factor of 2, a fact that was attributed to finite-size effects. The small number of dendrites likely also contributed to a faster transition between the stable states when compared to our results. It should be noted that a fast transition between states with significantly different mean primary spacing has also been associated with the cell-to-dendrite transition. However, our growth rates and thermal gradients are far from that transition as evidenced by the criteria suggested by Trivedi and Kurz $l_D = kl_T$ [21].

B. Ramping the rate of pulling speed

Experimental studies of the history dependence of primary spacing have focused on ramping the pulling speed slowly enough that the system is assumed to reach a steady state in between each ramping step of the velocity [6,7]. As an intermediate between this behavior and that found by us experimentally, we explore numerically a scenario whereby we ramp the pulling speed in discrete steps between 10 and 20 μm/s at different rates. This is achieved by varying the number ($N=2,5,10$) and duration of time intervals over which the pulling speed is kept constant before changing its value. The mean primary spacing is registered at the end of each interval. The results from these simulations are shown in Fig. 5. The starred data are obtained by starting from a morphologically noisy interface pulled at a constant speed of 10 μm/s until a statistically stable state is reached, and then using this configuration as an initial condition for a simula-

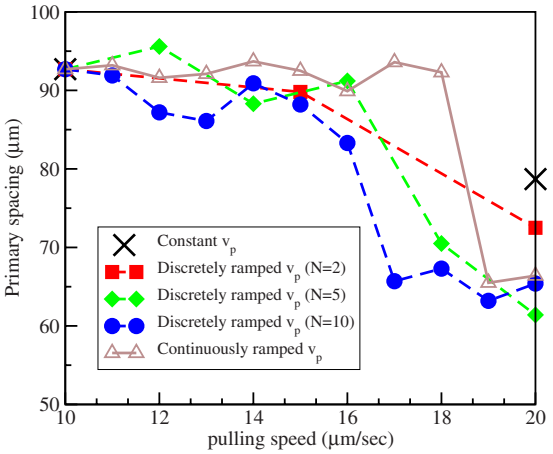

FIG. 5. (Color online) Spacing evolution versus pulling speed v_p as v_p is ramped from 10 to 20 μm in N time intervals, as well as continuously at each numerical time step; $G=5$ K/mm. The starred data are the mean steady-state spacing for the corresponding pulling speed. Depending on the particular growth conditions, the full width of the simulation domain, 4 mm, accommodates (in the case of larger spacing) more than 40 dendrite arms.

tion with a constant pulling speed of 20 μm/s until a new stable state is reached. The curves in Fig. 5 represent simulations starting with the same initial condition and taking an equal total amount of time t_{tot}, while the pulling speed is increased from 10 to 20 μm/s in N discrete steps such that the nth interval has a constant pulling speed of $v_p=10(1+n/N)$ μm/s and lasts t_{tot}/N. In an additional case the pulling speed is varied "continuously," namely, it is ramped at each iteration in the same way described above, taking N as the total number of iterations required for the simulation to last t_{tot}.

It is noteworthy that Figs. 4 and 5 exhibit the same qualitative behavior for the time evolution of the mean spacing, even though the control parameters in these two figures cover very different ranges of pulling speed and thermal gradient and begin with very different initial conditions. As mentioned above, the general behavior is consistent with the theory of Langer and Warren and the experiments of Losert *et al.*, and it points to the fact that dendritic arrays are stable over extended ranges of solidification rate, at least under transient conditions.

The transient data of Fig. 5 show that competitive growth between neighboring cells is negligible during periods where the mean spacing remains roughly constant, while it dominates the evolution of the array during the transition between those states. To explain this we note that the creation of new dendrites, or the elimination of existing ones due to competitive growth, is not instantaneous but requires some characteristic time. Even in an ideal periodic array, transitions between stable states will occur over some time. A distribution of spacings will thus shift its mean value gradually, which will result in an extended transition period. As the pulling speed increases, the distribution of primary spacings remains roughly unchanged, until a critical velocity is exceeded. At this point wavelengths in the distribution larger than some maximum value become most unstable to competitive

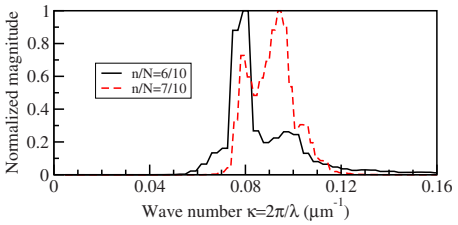

FIG. 6. (Color online) Shift of the main peak of the power spectra of a dendritic array as v_p is increased from a lower (continuous black line) to higher (dashed red line) value of v_p. It is evident that larger wavelengths in the early time shift to shorter wavelengths at later time, when v_p is increased. These power spectra correspond to the transition period during the seventh interval in the simulation with $N=10$ ramping steps shown in Fig. 5.

growth and tip splitting, and cell readjustment occurs. The weight of the spacing distribution shifts toward a smaller mean spacing (i.e., higher frequency). This is illustrated in Fig. 6. During discrete increments in the pulling speed, it is expected that entire ranges of spacings will be affected at each step. As the pulling speed is increased further, shorter wavelengths are affected until another critical pulling speed is reached when all wavelengths have been affected, after which the system stabilizes into a new stable state characterized by a smaller mean spacing. Figure 7 shows the power spectra corresponding points in the last interval in the simulation with $N=10$ ramping steps in Fig. 5, exemplifying the statistical stability of the spacing distribution during the incubation periods.

The mechanism discussed above depends on the applicability of the theory of Warren and Langer to an array with a distribution of primary spacings. In that case, the critical values of pulling speed are expected to depend in some as yet unknown way on the rate of change of pulling speed. However, the proposed mechanism is consistent with the analytical expressions for the critical values of pulling speed that have been proposed by Ma [22].

With regard to thermal gradient, we expect that given its stabilizing effect a larger thermal gradient would reduce not only the average spacing but also the spread (in absolute values) of the spacings present in the array. Thus, we would expect a reduction in the duration of the transition periods, and accordingly different critical values of the pulling speed limiting the transition, not because of a change in how the pulling speed affects different wavelengths but because less

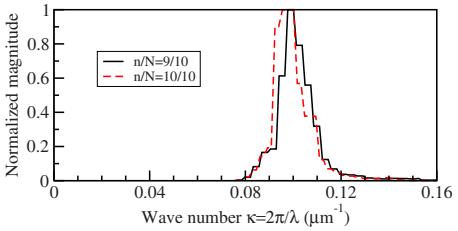

FIG. 7. (Color online) Power spectra of the dendritic array during two stages of the incubation period corresponding to the last interval in the simulation with $N=10$ ramping steps illustrated in Fig. 5.

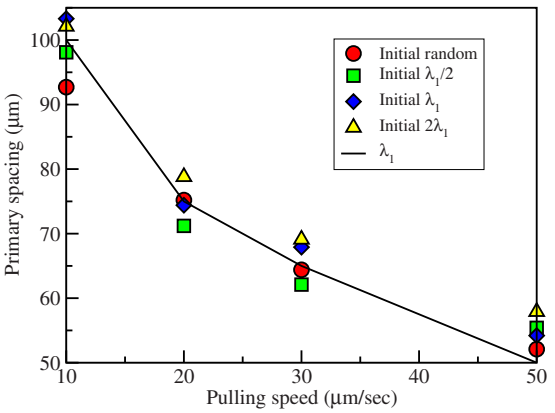

FIG. 8. (Color online) Primary spacing for different morphologically distinct initial interfaces, where λ_1 approximates the mean spacing registered when starting form a morphologically noisy interface. The other data sets correspond to the spacing reached from initial interfaces with a sinusoidal perturbation corresponding to the harmonic of λ_1 indicated.

wavelengths are present in the array. In the same way, we expect the initial state of the system (growth conditions, initial concentration distribution, and morphology of the interface) to affect the values of the critical pulling speeds that limit the transition periods by influencing the initial spectrum of wavelengths composing the array.

Figure 5 suggests that the higher the rate of change of v_p (larger N), the shorter lived is the unstable growth regime. This may be due to the fact that the shorter the time between step changes in v_p (t_{tot}/N), the longer a particular wavelength remains stable against splitting or merging. As a result, a particular v_p is eventually attained where a large number of wavelengths simultaneously become unstable, leading to an abrupt change in mean spacing. Conversely, the longer the interval between steps (lower N), the more time each wavelength in the system has to become unstable in accordance to the current v_p. When that is the case, the evolution becomes more monotonic and closer to the predictions for steady-state growth (starred data in Fig. 5).

C. Initial conditions and history dependence

The accumulated evidence on the history dependence of the morphology of an extended array in a stable state presents an opportunity to extend our numerical study of transient growth conditions. Figure 8 plots the mean primary spacing λ_1 once a stable state is reached for a constant v_p, for different initial interface morphologies. One set of λ_1 vs v_p consists of starting from a morphologically noisy flat interface, which is the same as the case previously examined by Greenwood *et al.* [12]. In the data sets, the initial conditions consist of an initially sinusoidal interface of wavelength half, equal, and double the value of the spacing $\lambda_1(v_p)$, i.e., the mean spacing of the stable state reached under random initial conditions. The results show certain dispersion in the final spacing, but are nonetheless confined within a narrow band. The dispersion in Fig. 5 is larger than the band size in Fig. 8 at the same velocity (see, for example, 20 μm/s). This is

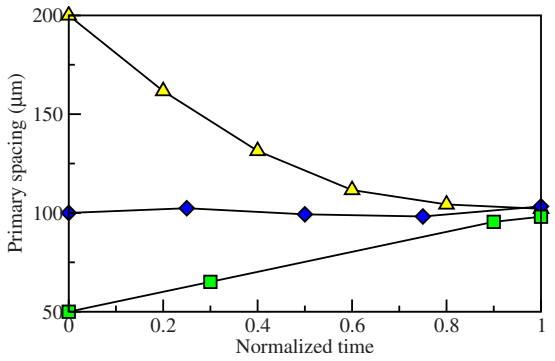

FIG. 9. (Color online) Evolution of the spacing when $v_p = 10$ μm/s from three different initial spacings λ_{init} corresponding to each curve; $G=5$ K/mm.

because the spacings in Fig. 5 did not have enough time to converge toward the stable band predicted in Fig. 8. The convergence of the mean spacing, for a fixed v_p, is illustrated in Fig. 9. If this is a general feature of convergence, it would imply that a large enough spread in the initial conditions will lead to a mean spacing that asymptotically falls within a progressively narrowing band of values. When the evolution of the system is interrupted before reaching convergence, as when ramping the pulling speed or under transient conditions, the width of the band within which the spacing falls will depend on the proximity of the (evolving) band to its converged values. The broader the distribution of initial states, the longer the system is expected to require to approach stability.

Further insight into the history dependence and transient evolution of primary spacing can be found in the sets of simulations summarized in Fig. 10. Each set corresponds to a series of simulations with (different) constant pulling speed, where the state reached at the end of a simulation serves as

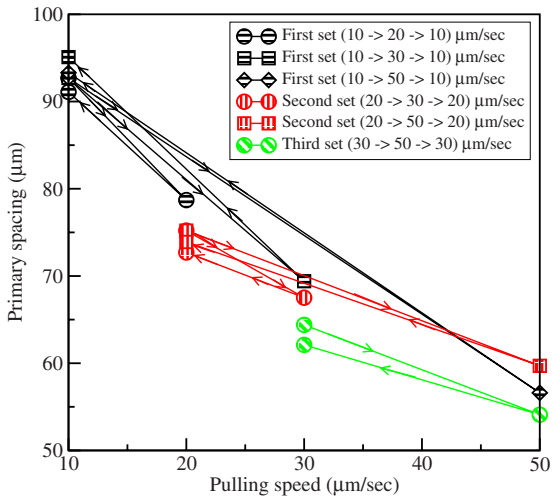

FIG. 10. (Color online) Mean spacing registered once the system stabilizes under different constant pulling speeds, for sets of simulations where the stable state reached at the end of a simulation serves as initial condition for the next one. The first simulation in each set starts with a flat interface roughened by adding morphological random noise; $G=5$ K/mm.

the initial condition for the next one. The first simulation in each set starts with a flat interface roughened by adding morphological random noise. In the set connected by black arrows, the first simulation has a constant pulling speed of $v_p = 10$ μm/s. Once the system reached stability, the resulting state served as the initial condition for three simulations with different constant pulling speeds of $v_p = 20$, 30, and 50 μm/s. When stability is reached in each of these cases, each of the resulting stable configurations ($v_p = 20$, 30, and 50 μm/s) serves as an initial condition for simulations where the pulling speed is set (back) to a constant value of $v_p = 10$ μm/s. The second and third sets in Fig. 10, each interconnected by (red and green) arrows, follow an analogous procedure. The second set starts with $v_p = 20$ μm/s, the result of which serves as the initial condition for simulations with constant pulling speeds of $v_p = 30$ μm/s and $v_p = 50$ μm/s, respectively. Each of these results then serves as the initial condition for two simulations where the pulling speed is set (back) to a constant value of $v_p = 20$ μm/s. The third set starts at $v_p = 30$ μm/s, the result of which serves as the initial condition for simulations with a pulling speed of $v_p = 50$ μm/s, the result of which, in turn, serves as the initial condition for simulations where the pulling speed is set back to $v_p = 30$ μm/s.

Figure 10 exhibits the same qualitative behavior as Fig. 8, both presenting an apparent tight band of accessible mean spacings. It is noteworthy that the limits of the apparent bands in Figs. 8 and 10 are very similar since the stable states have been reached in both cases.

IV. CONCLUSIONS

Under transient conditions, our work shows that the power-law behavior predicted by most previous heuristic models is incorrect. In fact, under transient conditions the mean spacing appears relatively stable over a broad range of pulling speeds, changing relatively rapidly at specific values, which depend on the rate of change of the pulling speed. Even in the case of transient dendritic growth the concept of a predictable description of spacing within the confines of a phase space attractor of dendrite spacings that is mathematically—or at least numerically—calculable may still be plausible. As our results indicate, such an analysis would have to incorporate the time dependence of velocity and its effect on where rapid changes between stable states occur. Further study is required to go beyond the current geometrical models. The results of simulations and experiments suggest that a natural theoretical framework for a spacing selection theory under transient conditions would start by extrapolating the dynamical stability theory of Warren and Langer to include a dendritic array with a *distribution* of wavelengths.

While hysteresis in spacing evolution was not investigated explicitly, Fig. 10 seems compatible with that a set of simulations in which the pulling speed is cycled, say through $(10 \rightarrow 20 \rightarrow 30 \rightarrow 50 \rightarrow 30 \rightarrow 20 \rightarrow 10)$ μm/s, may present hysteresis within at least a closed band when plotted in terms of the average spacing vs pulling speed. However, we do not have enough evidence to conclude that the average spacing will cycle if the pulling speed is cycled. We also find observationally that the effects on the morphology of a dendritic array, and in particular the average spacing of the system, often lag behind its causes. This can influence, for example, the distribution of modes comprising an array and the resulting characteristic time over which their destabilization occurs to shift in the mean spacing of the array. Ultimately, this effect can create a hysteresis on not only the velocity but also the duration of the transition period between spacing branches.

It is noteworthy that the study of morphology selection, and in particular spacing selection in extended dendrite arrays, has been increasingly regarded as a practical "materials" problem and relegated to journals dedicated to pragmatic problems. This has been in part due to the fact that appropriate fundamental formalisms, such as the phase-field method used in the present paper [10], have only become available relatively recently. Our work here demonstrates that spacing selection in solidification in fact possesses many open fundamental questions regarding nonequilibrium pattern formation in extended driven systems. It is hoped that our work will peak interest in and lead to further studies in this important paradigm of nonequilibrium pattern formation.

ACKNOWLEDGMENTS

We thank Nana Ofori-Opoku and Michael Greenwood for their significant contribution to the development of the numerical codes employed in this work. We thank the National Science and Engineering Research Council of Canada (NSERC), Novelis Global Technology Centre, and the Canadian Space Agency (CSA) for financial support.

[1] K. Somboonsuk, J. T. Mason, and R. Trivedi, Metall. Trans. A **15A**, 967 (1983).
[2] D. Bouchard and J. S. Kirkaldy, Metall. Mater. Trans. B **28**, 651 (1997).
[3] J. D. Hunt, *International Conference on Solidification and Casting of Metals* (The Metals Society, London, 1979), p. 3.
[4] J. A. Warren and J. S. Langer, Phys. Rev. A **42**, 3518 (1990).
[5] J. A. Warren and J. S. Langer, Phys. Rev. E **47**, 2702 (1993).
[6] X. Lin, W. Huang, J. Feng, T. Li, and Y. Zhou, Acta Mater. **47**, 3271 (1999).
[7] W. Losert, B. Q. Shi, H. Z. Cummins, and J. A. Warren, Phys. Rev. Lett. **77**, 889 (1996).
[8] W. J. Boettinger and J. A. Warren, J. Cryst. Growth **200**, 583 (1999).
[9] A. Karma, Phys. Rev. Lett. **87**, 115701 (2001).
[10] B. Echebarria, R. Folch, A. Karma, and M. Plapp, Phys. Rev. E **70**, 061604 (2004).
[11] N. Provatas, N. Goldenfeld, and J. Dantzig, Phys. Rev. Lett.

80, 3308 (1998).
[12] M. Greenwood, M. Haataja, and N. Provatas, Phys. Rev. Lett. **93**, 246101 (2004).
[13] N. Provatas, M. Greenwood, B. Athreya, N. Goldenfeld, and J. Dantzig, Int. J. Mod. Phys. B **19**, 4525 (2005).
[14] S. Gurevich, A. Karma, M. Plapp, and R. Trivedi, Phys. Rev. E **81**, 011603 (2010).
[15] H. Wang, Ph.D. thesis, McMaster University, 2009.
[16] B. Echebarria, A. Karma, and S. Gurevich, Phys. Rev. E **81**, 021608 (2010).
[17] A. Karma, Phys. Rev. E **48**, 3441 (1993).
[18] B. P. Athreya, N. Goldenfeld, J. A. Dantzig, M. Greenwood, and N. Provatas, Phys. Rev. E **76**, 056706 (2007).
[19] M. Amoorezaei, S. Gurevich, and N. Provatas, Acta Mater. **58**, 6115 (2010).
[20] J. D. Hunt and S. Z. Lu, Metall. Mater. Trans. A **27**, 611 (1996).
[21] R. Trivedi and W. Kurz, Int. Mater. Rev. **39**, 49 (1994).
[22] D. Ma, Metall. Mater. Trans. B **33**, 223 (2002).